

Online, Feature Stacking (FEAST) Based “Channel + Beam” Handoff Control in Cognitive Radio Networks with Multi-Beam Antennas

Koushik A M*, Fei Hu*[†], and Sunil Kumar[‡]

*Electrical and Computer Engineering, The University of Alabama, USA ([†] Corresponding author)

[‡]Electrical and Computer Engineering, San Diego State University, San Diego, CA, USA

Abstract—A novel Feature Stacking (FEAST) based “channel + beam” handoff (CBH) control scheme is proposed for the cognitive radio networks (CRNs) with multi-beam smart antennas (MBSAs). Spectrum handoff uses the mixed Preemptive/Non-preemptive M/G/1 queueing model with a discretion rule in each beam, to overcome the interruptions from the primary users (PU) and the channel contentions among different classes of secondary users (SUs). A real-time CBH scheme is designed in which the packets in an interrupted beam of a SU can be detoured through its neighboring beams. The percentage of packets detoured on a beam is determined based on the beam’s available capacity and queue size. A novel, online supervised learning scheme (known as FEAST) based CBH algorithm is also proposed to maximize the Quality of Experience of user data in the long term. The FEAST-based CBH scheme adapts to the dynamic channel conditions and performs spectrum decision in time- and space-varying CRN conditions. The simulation results demonstrate the effectiveness of our CBH-based packet detouring scheme and show that the proposed FEAST-based spectrum decision can adapt to the complex channel conditions and improves the quality of video transmissions compared to the unsupervised learning based handoff schemes.

Index Terms—Spectrum Handoff, Cognitive Radio Networks (CRNs), Queueing, Multi-Beam Smart Antennas (MBSAs), Preemptive (PRP)/Non-Preemptive (NPRP), Machine Learning.

I. INTRODUCTION

In this paper, we study the handoff issues in cognitive radio networks (CRN) where the wireless nodes are equipped with multi-beam smart antennas (MBSAs). The secondary users (SUs) use the licensed spectrum opportunistically whenever the licensed user (i.e., a primary user (PU)) is not active. Hence, CRNs need a smart spectrum decision scheme to timely switch the channels [1]. An important issue in spectrum decision is spectrum handoff. Since the SU’s spectrum usage is constrained by the PU’s traffic pattern, it should carefully choose the right handoff time. On the other hand, the user mobility introduces the time- and space-varying channel conditions, which make the spectrum handoff challenging.

The use of directional antennas, especially MBSAs [2], can significantly enhance the wireless transmission performance. Unlike the omnidirectional transmission that needs more transmit power and causes interference to the neighboring nodes, a directional antenna can transmit data towards an intended receiver over a long range and the beam angle can be adjusted so that it does not interfere with its neighboring nodes. This also enables the spatial reuse leading to higher network

throughput. In a CRN consisting of the nodes equipped with MBSA, each beam can occupy a different channel at the same time to reduce the interference with the PUs [2]. However, the half-duplex nodes equipped with MBSAs do have one constraint - all beams should be in either all-Tx (transmission) or all-Rx (reception) mode at any given time [2].

If the channel being used by an antenna beam of a SU is occupied by a PU, the beam can either switch to another channel or its traffic can be sent via other beam(s) of the node. We call the former as the “channel handoff”, and the latter as the “beam handoff”. Together they are called as the “channel + beam” handoff (CBH). In [3], we briefly discussed the following three issues related to CBH: 1) *Multi-class handoff* to handle PU or SU interruptions, based on a mixed PRP/NPRP M/G/1 queueing model with a discretion rule [4]. 2) *Multiple handoff decisions*: When a beam of SU is interrupted by a PU or a higher priority SU, three handoff options are available: (a) stay-and-wait, (b) channel switching, and (c) beam handoff. 3) *Throughput-efficient beam handoff* to select the detour paths by considering the channel capacity and queue size of each beam. In this paper, the beam handoff process of forwarding the data of an interrupted beam via other beam(s) of the node is also known as the packet detouring and the paths taken by those packets are known as the detour paths.

This paper significantly extends our preliminary results in [3] as discussed below.

First, we study the beam handoff and solve the packet detouring issue through an optimal rate allocation scheme among the available neighbor beams. When any beam of a SU with MBSA is interrupted, its source data is shared among neighboring beams based on their channel capacity and buffer levels. The nodes which are one-hop away from both the sender and receiver are used for packet detouring. We formulate the packet detouring as an optimization problem to achieve the desired QoS level. Our optimization model considers detouring beam’s own data flows, channel capacity, and queue level.

Second, we extend the time-domain spectrum handoff to a complete spectrum decision model by using queueing theory. We also consider the space-varying characteristics of SUs such as the mobility-caused multi-path fading, which introduces significant variations in the packet error rates (PERs) and affects the QoS. The SU collects the network parameters (e.g., handoff delay, channel status, and PER etc.) to make

the spectrum handoff decision during the interruption. The spectrum decision performance is measured in the Mean Opinion Score (MOS).

Third, we propose a supervised learning-based scheme to achieve CBH in dynamic channel conditions. Existing intelligent spectrum decision schemes in CRNs use the unsupervised learning to improve the long-term performance. For example, the reinforcement learning (RL)-based unsupervised learning scheme uses the Markov Decision Process (MDP) to build the optimal spectrum decision model over the long term [1]. Since the CRN conditions are dynamic due to the user mobility, multipath fading, and channel conditions, the learning models should be able to learn the radio environment on the fly. Moreover, since the arrival time of a PU or a high-priority SU is random, the SU node cannot afford to spend much time in learning the spectrum handoff strategies.

Therefore, we propose a no-regret online learning model, called FEAST (*Feature Stacking*), which takes the appropriate spectrum decision on the fly by mapping the observed CRN features to one of the optimal classifiers of support vector machine (SVM). Specifically, the Rapid Response Engine (RRE) takes the rapid decisions as a short-term handoff control policy based on the previously built learning model. When the observed spectrum handoff performance falls below a threshold, the node invokes the Long Term Response Engine (LTRE), which collects the current CRN features, adds them to the old feature set, and updates the model as a long-term handoff control policy, which is then transferred to RRE. Thus FEAST can learn and adapt to the dynamic CRN channel conditions on the fly by adding the newly observed radio characteristics to the dataset for improving the spectrum decision accuracy in each iteration. Figure 1 illustrates the FEAST based spectrum decision model.

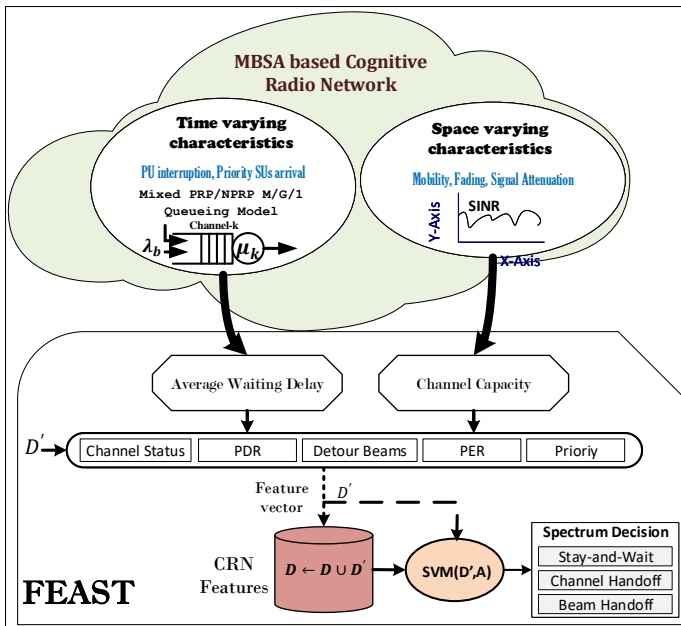


Fig. 1: FEAST “Channel + Beam” spectrum handoff model in MBSA-based CRNs.

The rest of this paper is organized as follows: The related work is discussed in Section II. The network model used

in this paper is described in Section III, followed by the queueing model in Section IV. The beam handoff principle via beam detouring is discussed in Section V, followed by the FEAST-based CBH in Section VI. Section VII describes the performance of the proposed handoff schemes, followed by the conclusions in Section VIII.

II. RELATED WORK

A. Parallel and Independent Queueing Model for Networks with Directional Antennas:

Only few schemes have addressed the scheduling issues in directional communication systems. A distributed scheduling algorithm based on queue length changes during the past time slots was presented in [5]. The stability of this algorithm is analyzed through a mean drift analysis. In [6], an optimum scheduling was proposed for a multi-antenna UAV central node, which collects channel state information from multiple distributed UAVs, and the optimum beam scheduling problem is solved via beamforming.

The above-mentioned schemes consider only general directional antennas, and not the MBSA-based CRNs. In our pioneering work on MBSA-based CRNs, a non-preemptive resume priority (NPRP) M/G/1 queueing model was proposed in [7], where the high priority node cannot interrupt low priority nodes being served. The drawback of this model is that high priority users with low latency traffic may suffer from long queueing delay, which eventually degrades the user’s quality-of-experience (QoE). A preemptive resume priority (PRP) M/G/1 queueing model was proposed for CRNs with multi-priority SU connections in [8]. This model gives ample spectrum access opportunities to high priority users, but the low priority SUs can experience multiple interruptions. Recently, we proposed a mixed PRP-NPRP M/G/1 queueing model in [9]. If the remaining service time of an SU is above a predefined threshold, it operates in the PRP mode; otherwise, it operates in the NPRP mode. In this paper, we use the mixed PRP/NPRP M/G/1 queueing model, by considering the multi-beam queueing service time as a discretion rule and by formulating a parallel and independent queueing model for SU with MBSA.

B. Packet Detouring in CRNs:

A packet detouring scheme based on the link quality observations in a diamond-like network topology was presented in [3]. It considered the 2-hop communication in a Rayleigh fading channel for omni-directional communication. A QoE-oriented relay scheduling problem in CRNs was studied in [10] to ensure the optimized performance in terms of high capacity and low packet loss rate. It detours the packets through multiple neighboring nodes when there is an interruption from the PU. Similar work was done in [11] where beamforming was used among the relay nodes, PUs, and other SUs, to determine the channel state information (CSI) to detour the packets upon the interruption from PUs. However, all the existing schemes on packet detouring in CRNs consider the interruptions from the PU only, without considering the multi-SU contention. In this paper, the packet detouring is used

whenever there is an interruption from a PU or high priority SU, and the packets are detoured only for the interruption time interval, which is determined by using the mixed PRP/NPRP M/G/1 queueing model with a discretion threshold.

C. Spectrum Handoff:

In our previous works [1], [7], [9], [12], we designed the RL-based spectrum handoff schemes by considering the channel status (measured by PDR), channel quality (measured by PER), and the SU priorities. The main drawback of the Markov decision based RL model is that it needs many iterations to converge to an optimal solution, which is not affordable in the network where the channel access time is very limited. Another limitation of these approaches is that they cannot adapt to the channel variations on the fly. The proposed FEAST-based spectrum decision model learns and acts according to the complex channel conditions on the fly, through the SVM-based learning model. A few other schemes have also used the SVM for spectrum handoff. Authors in [13] presented a SVM-based spectrum handoff scheme where the nodes can predict the handoff time proactively before the channel is occupied by the PUs. However, the scheme does not consider different channel characteristics (PDR, PER, etc.) before switching the channel. In [14], the proposed spectrum mobility prediction was used by considering the time-varying channel characteristics. However, such a learning scheme cannot be performed on the fly.

III. NETWORK MODEL

We assume a CRN consisting of n SUs equipped with MB-SAs. The directional antenna can form beams in M sectors (see Fig 2) with each sector having a beamwidth of $\frac{360}{M}$ degrees. The sectorization provides higher interference suppression and efficient frequency reuse.

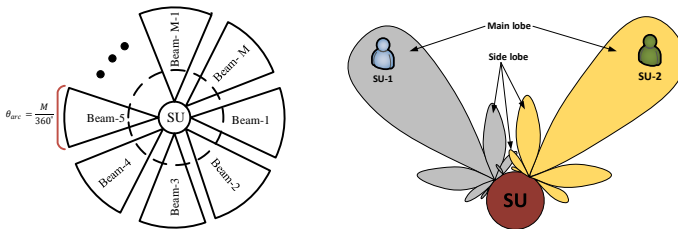


Fig. 2: Multi-beam sector antenna model (left) and Multi-beam antenna lobes (right).

We assume a network where each beam of multibeam equipped SU can occupy a different channel. Through each beam, the SU communicates with a different SU in the network. Without the loss of generality, we consider that the sender SU can reach out to the receiving SU through direct transmission or over a 2-hop path through relay node(s). Each relay node also has its own data to transmit to other nodes in the network.

IV. QUEUEING MODEL WITH DISCRETION RULE

We consider an MBSA with M beams that can handle independent flows. Figure 3 shows the schematic diagram of a

queueing model with the use of MBSA. Each beam maintains a queue with packet arrival rate λ_b (arrivals/slot) and mean service rate X_b (slots/arrival), $b \in \{1, 2, \dots, M\}$. These queues are analyzed individually through the mixed PRP/NPRP M/G/1 queueing model [9]. We assume K flows ($K \leq M$) are sent to different SUs at time instance t , where the associated signal vector can be represented as $s(t) = [s_1(t), s_2(t), \dots, s_K(t)]^T$.

In addition, we assume that there are N randomly located neighbors around the SU. Each beam of the SU selects an appropriate channel with long channel holding time and high signal to interference and noise ratio (SINR). All the beams can select the same or different channels since the interference between the adjacent beams is assumed to be negligible in a MBSA. These beams can transmit different types of traffic packets with various priority levels. The SU beam containing the packets with the smallest delay deadline is assigned the highest priority ($j = 2$) (note that $j = 1$ is reserved for PU), whereas the beam serving the packets with the longest delay deadline is assigned the lowest priority ($j = C$). Note that the channel selected by a beam may be interrupted due to the arrival of the PU or higher-priority SUs' traffic.

In the PRP queueing scheme, the lower priority SU's service can be interrupted at any time by a PU or a higher priority SU. On the other hand, the service of the low-priority SU cannot be interrupted by a higher priority SU in the NPRP model. Our queueing scheme uses the mixed PRP/NPRP model with a discretion rule, based on the remaining service time of the low priority SU [9]. We assume that the interrupted SU can resume its transmission from the point where it was interrupted as soon as a channel becomes available. Figure 3 depicts the mixed PRP/NPRP M/G/1 queueing model for a SU with MBSA.

We classify the CRN nodes, which are using a given channel, into three classes [15]: type α , j and β . Type α includes any PU or higher priority SUs, $1 \leq \alpha \leq j-1$. Type j refers to the SUs with priority j , and a Type β SU has a priority β , $j+1 \leq \beta \leq C$. Type β users can be in protective mode based on their remaining service time. Hence, a newly joined type j SU on a channel (or a SU which has been handed off to this channel) has to wait in the queue if there is any higher priority user (or a user in the non-preemptive mode) ahead of it in the queue; otherwise, it can immediately take over the channel.

Discretion Rule: To reduce the queueing delay (which is the major part of the handoff delay) of a low-priority SU, we adopt a discretion rule which does not allow its transmission to be interrupted if its remaining service time is below a threshold (i.e., on the verge of completing its service) [9]. The total service time of an SU, S_j , is determined by the preemptive duration S_{A_j} and the non-preemptive duration S_{B_j} [9]:

$$S_j = S_{A_j} + S_{B_j} \quad (1)$$

For a threshold, τ_j , the discretion rule can be defined by

$$S_{A_j} = \max[0, S_j - \tau_j] \text{ and } S_{B_j} = \min[S_j, \tau_j] \quad (2)$$

For a PU, we have $S_{B_1} = 0$ and $S_{A_1} = S_1$ since it is allowed to interrupt any SU.

Spectrum Handoff Delay: We define the type j connection as the secondary connection that has experienced i interrup-

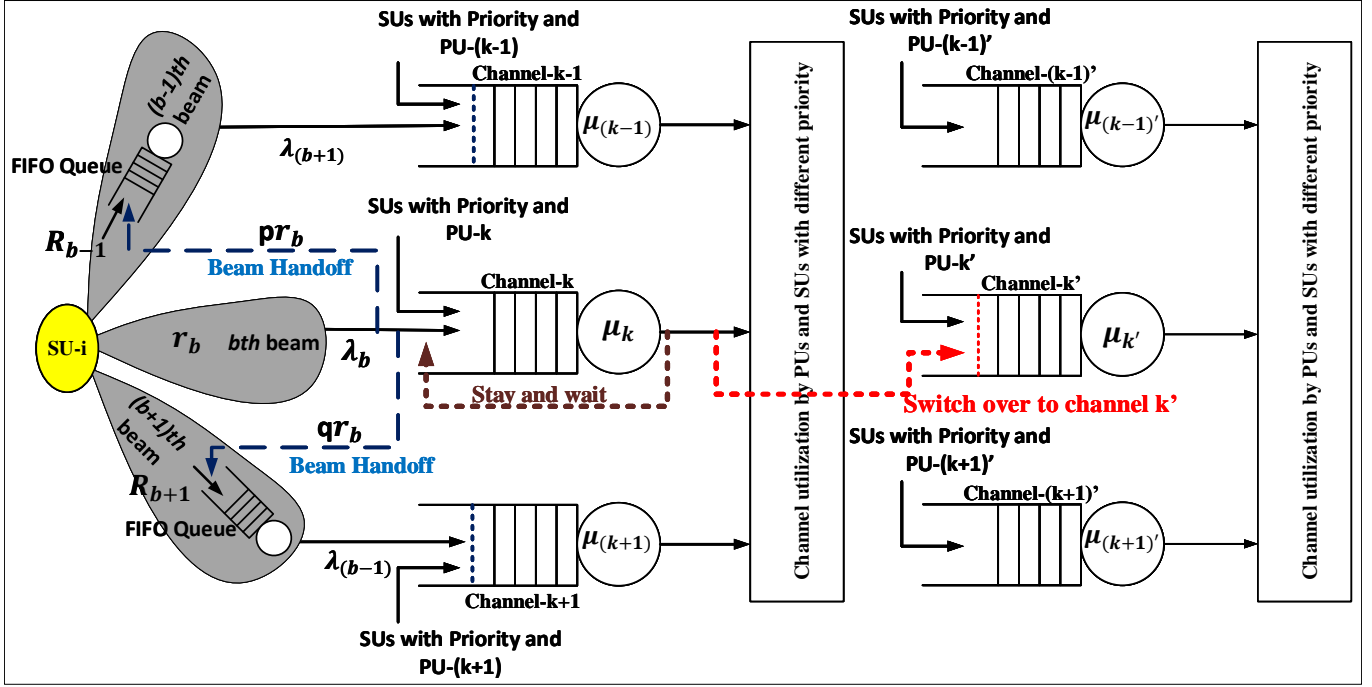


Fig. 3: Queuing model in CRNs with MBSAs.

tions, $0 \leq i \leq n_{max}$, where n_{max} is the maximum allowable interruptions. When the beam b_j of an SU, using channel k , is interrupted by a high-priority user, it may either stay in the same channel and wait for it to become available again (known as the stay-and-wait case) or move to another channel k' (known as the channel switching case), depending upon the channel switching time and channel holding time.

The handoff delay $E[W'_{ji}^{(k)}]$, starting from the instance of i^{th} interruption to the instance when the interrupted service is resumed in channel k , can be determined as [9],

$$E[W'_{ji}^{(k,b)}] = \begin{cases} E[W'_j^{(k)}], & \text{if stay-and-wait in channel } k \\ E[W_j^{(k)}] + T_s, & \text{if switches from channel } k \text{ to } k' \end{cases}$$

Here, $E[W'_j^{(k)}]$ (or $E[W_j^{(k)}]$) is the average delay of the i^{th} interruption, if the interrupted beam of SU chooses to stay at the same channel k (or switch over to channel k'). T_s is the channel switching time assumed to be known beforehand. The detailed expressions for computing the handoff delay for both cases are available in [9]. For simplicity, the average queuing delay, $E[W'_{ji}^{(k,b)}]$ of the interrupted beam is denoted as $E[W]$ in the rest of this paper.

V. BEAM HANDOFF VIA PACKET DETOURING

During the spectrum handoff, the interrupted beam of an SU may stay idle when it is either in the stay-and-wait mode or its packets are waiting in the queue during the channel handoff. The proposed beam handoff scheme can eliminate or reduce this waiting/queuing delay by allowing the data packets of the interrupted beam to be detoured to the destination through the neighboring beams of the node. Let \tilde{N} represent the number of available detour beams that form a parallel queuing system.

Figure 4 shows a typical packet detouring scenario among \tilde{N} neighboring beams of SU. In addition to detouring the packets

from other beams, each detour beam also has its own data packets to be sent to the next-hop node or destination. The packets in the queue of a beam are served using first-in-first-out (FIFO) order. Recall that all the beams of an SU should be synchronized, i.e., all the beams should either send or receive the packets at a given time. Without the loss of generality, we assume in Fig. 4 that the traffic of the interrupted beam of the source node S (which was connected to the destination node D via a 1-hop link before interruption) is detoured by using its other beams which are connected to the destination D through the 2-hop links via relay nodes. In practice, the detour beams can also use more than two hops.

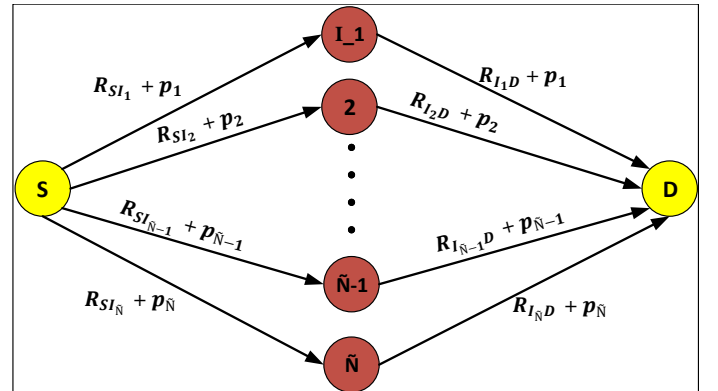


Fig. 4: Detouring path: distribution of packets among different beams in a 2-hop relay.

For a 2-hop detour path (e.g., $S - I_i - D$) in Fig. 4, the source SU S is in the transmission mode (Tx) and the relay SU I_i is in the reception mode (Rx) in the first phase. In the second phase, the I_i is in Tx mode and D is in the Rx mode. Here, additional delay is introduced due to the use of 2-hop paths through the relay nodes. Therefore, the aggregate data rate at

the relay node I_i can be given by:

$$R_{agg,S I_i} = R_{S I_i} + p_i \text{ bits/sec for } i \in \{1, 2, \dots, \tilde{N}\} \quad (3)$$

The aggregate data rate at D from the relay node I_i can be given by:

$$R_{agg,I_i D} = R_{I_i D} + p_i \text{ bits/sec for } i \in \{1, 2, \dots, \tilde{N}\} \quad (4)$$

where, $R_{S I_i}$ is the own data rate of the source S to the relay node I_i and $R_{I_i D}$ is the own data rate of the relay node I_i to the destination D , on beam i . We assume that r_b is the source data rate on the interrupted beam b that will be sent to the destination D through the detour beams. p_i is the fraction of r_b that can be detoured through beam i and $i \neq b$, $i \in \{1, 2, \dots, \tilde{N}\}$. Hence, (3) and (4) represent the traffic load on each link.

Our goal is to compute the value of p_i that can be transmitted over the detour path i . Since the channel conditions of a link are instantaneous and its corresponding transmission rate may not meet the current application requirements, each link can have outage and all the packets to/from the relay SU may not be detoured successfully. The SINR observed at beam b for the channel k can be written as [12],

$$SINR_{k,b} = \frac{(1/n_k)|h_k u_b|^2}{\sigma^2 + \sum_{i \neq b}^{n_k} (1/n_k)|h_k u_i|^2} \quad (5)$$

Where n_k denotes the number of neighboring beams, h_k denotes the gain in channel k , and u_b (or u_i) denotes the unit power assigned to beam b (or i where $i \neq b$). The link capacity associated with the detour beam i , for the $SINR_{k',i}$ and bandwidth B in channel k' , is defined as

$$C_i = B * \log_2(1 + SINR_{k',i}) \text{ bits/sec for } i \in \{1, 2, \dots, \tilde{N}\} \quad (6)$$

Thus the maximum available link capacity in the detour link i is

$$C_i = \min(C_{S I_i}, C_{I_i D}) \text{ bits/sec for } i \in \{1, 2, \dots, \tilde{N}\} \quad (7)$$

Since it is assumed that each detour beam also has its own data to send, the minimum capacity required for the successful transmission of detour beam's own data in link i is

$$R_i = \max(R_{S I_i}, R_{I_i D}) \text{ bits/sec for } i \in \{1, 2, \dots, \tilde{N}\} \quad (8)$$

Where $R_{S I_i}$ ($R_{I_i D}$) is the detour beam's own data rate on detour path i .

On a 2-hop path, an SU has to switch from Tx to Rx mode, and *vice versa*, during the available transmission period ($E[W]$). Since the MBSA beams are synchronized, we assume that each detour path has equal Tx and Rx durations. Therefore, the fraction of the maximum data that can be detoured on path i over two hops is

$$p_{C_i} = \frac{1}{2} \left[1 - \frac{R_i}{C_i} \right] \text{ for } i \in \{1, 2, \dots, \tilde{N}\} \quad (9)$$

In (9), the control packet overhead and the transmission mode switching delay are ignored. Each detour beam has an independent queue to serve the data packets. The detoured packets, together with the original packets, will increase the packet accumulation level in the buffer. Therefore, the number of packets that can be detoured on a beam should be selected such that the buffer does not overflow. We assume that the

maximum buffer size of a beam is L packets. The buffer level at beam i due to its own traffic at any instance, t , can be computed as

$$L_i = \frac{R_i}{L_p} \times E[W_i] \times L_t, \quad i \in \{1, 2, \dots, \tilde{N}\} \quad (10)$$

where R_i is from (8), L_p is the packet length, L_t length of the time slot and $E[W_i]$ is the average queuing delay in path i (from the FIFO queue of beam i). To avoid the packet drops due to buffer overflow, L_i should be less than L . Let PDR_i be the total packet dropping rate observed at the detour path i , then the fraction of data rate of beam b that can be detoured on link i is

$$p_i = (1 - PDR_i) * p_{C_i} * r_b \text{ bits/sec, for } i \in \{1, 2, \dots, \tilde{N}\} \quad (11)$$

For successful packet detouring, an optimization procedure for determining the detour path with the maximum achievable throughput can be expressed as

$$\begin{aligned} & \max MOS_b \\ & s.t: i. \quad \sum_{i=1}^{\tilde{N}} p_i \leq r_b, \\ & \quad ii. \quad C_i - R_i - p_i \geq 0, \\ & \quad iii. \quad (L - L_i)L_p \geq (C_i - R_i)L_t, \text{ for } i \in \{1, 2, \dots, \tilde{N}\} \end{aligned} \quad (12)$$

Here r_b is the source data rate of the interrupted beam, b which is supposed to be detoured, and R_i is the detour beam's own data rate, either from the source node to relay node, or from relay node to the destination node. The MOS [16] is used to measure the quality of data transmission (video or voice).

VI. FEAST-BASED CBH SCHEME

In this section, we address the intelligent spectrum decision using FEAST, an SVM based learning model that considers the multi-channel, multi-beam, and multi-SU (3M) scenario. When a new SU joins the network, it can make a spectrum decision by using the available time and spatial characteristics of the channel in beam b . Since the channel is time-varying, the previously learnt CBH model may not fit well at a new time instant, which would introduce the spectrum decision errors over time. Therefore, we propose a learning model which can make the optimal CBH decisions on the fly.

A. SVM-based Learning Model

The SVM is a supervised learning approach that has been applied to the data classification problems and regression analysis [14]. SVM is popular in statistical learning theory which adopts structural risk minimization principle, and has been shown to outperform the traditional neural network based classification [14], [17]. The SVM is very effective in high-dimensional spaces. Different kernel functions can be used in SVM, including the customized kernels. The training dataset consists of N_f pairs of input and output labels that can be represented as

$$(x_i, y_i), \quad i = 1, 2, \dots, N_f; x_i \in \mathcal{R}^d, y_i \in \mathcal{R}. \quad (13)$$

Here, x_i is the input vector containing multiple features, and $y_i \in [-1, +1]$ is the output data or class indicator. For

the training samples x_{i_t} at time instant t with $t = 1, 2, \dots, T$, the SVM maps the inputs to outputs and predicts an output $[-1, +1]$ (for a 2-class problem) by finding a hyperplane which has the maximum separation from the support vectors:

$$w \cdot x + c = 0 \quad (14)$$

with the largest margin satisfying the following conditions:

$$\begin{aligned} w \cdot x_{i_t} + c &\geq 1 \quad \text{for } y_{i_t} = 1 \\ w \cdot x_{i_t} + c &\leq -1 \quad \text{for } y_{i_t} = -1 \end{aligned} \quad (15)$$

Here, w is a vector perpendicular to the hyperplane which represents the hyperplane orientation, and $c = w_0$ represents the hyperplane position, also called as offset argument, which describes the perpendicular distance between the origin and hyperplane, as shown in Fig. 5. The main objective is to maximize the difference between the hyperplane and the support vectors of the two data classes, which is given by $\frac{2}{\|w\|}$. To avoid the overfitting and reduce the misclassification errors, we introduce a slack variable ξ_{i_t} [14], [18] to produce a classifier as,

$$y_{i_t}(w \cdot x_{i_t} + c) \geq 1 - \xi_{i_t}; \quad \xi_{i_t} \geq 0 \quad (16)$$

Here, $\xi_{i_t} = 0$ indicates that the dataset is correctly classified, and those data points are either on the margin or on the correct side of classification margin; $0 < \xi_{i_t} \leq 1$ means the dataset is inside the margin and correctly classified. To avoid the misclassifications (i.e., $\sum_{i_t} \xi_{i_t} > 1$), we can impose an upper bound on the number of training errors. Therefore, to achieve the minimum classification error, the distance between the support vectors (SVs) and the hyperplane should be maximum.

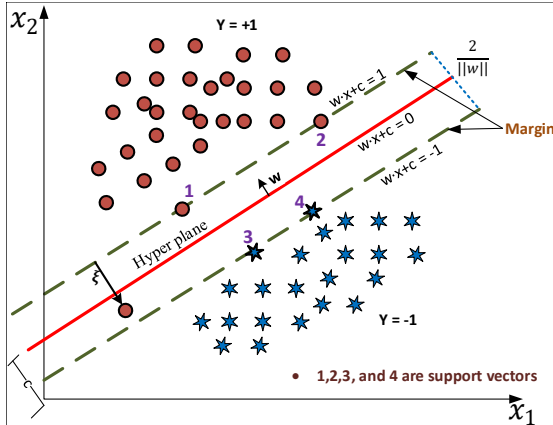


Fig. 5: Typical data classification using Support Vector Machine (SVM).

B. FEAST Learning Model

The machine learning is used in CRNs for building a cognitive system that can adapt to the dynamic RF environment. These cognitive systems rely on the accurate dynamic models, which can predict the long-term consequences of various spectrum decisions (actions) and suitable reward functions. But modeling an uncontrollable network environment is challenging. In addition, the previous models [1], [7], [9], [12] built for spectrum decision are mostly based on the assumption that the inputs (or observations) used in prediction follow the same

underlying distribution during both the training and testing phases. However, this assumption may not hold in dynamic RF environment, and can lead to poor QoS performance due to inaccurate spectrum decision in the long run. This situation would arise because a learned strategy (i.e., a specific action in a specific state vector (RF observation)) may not be robust to a different type of input or observation.

To overcome this issue, we propose the FEAST, which uses an online learning model. We represent each beam of SU in the CRN as a tuple denoted by $\langle D', A, R \rangle$, where:

a) *States, D'*: The states $S \in \mathcal{R}^d$ are called as the observations of CRN. In our model, the states in b^{th} beam of a SU consist of the following five aspects: (1) $\rho_b^{(k)}$ which represents the SU priority in b^{th} beam in channel k ; (2) Channel status $\chi_b^{(k)}$, i.e., whether the channel is occupied or idle; (3) Channel condition $v_b^{(k)}$, which determines the channel quality in terms of PER; (4) Traffic load on the channel, $\delta_b^{(k)}$, which is already determined in Section V in terms of PDR; and (5) The number of neighbor beams (\tilde{N}_b) for packet detouring in case of interruption. Collectively all the states can be represented as $D' = \{\rho_b^{(k)}, \chi_b^{(k)}, v_b^{(k)}, \delta_b^{(k)}, \tilde{N}_b^{(k)}\}$.

b) *Actions, A*: The actions are used to change the behavior of SU in response to the states. They are executed sequentially. If the states don't change significantly, the SU continues its operation in the current beam and channel. When the transmission of an SU is interrupted, the action set consists of the stay-and-wait at the current channel k , the spectrum handoff to another channel k' , and the beam handoff to detour the packets through the neighboring beams.

c) *Policy Set, π* : We denote the class of learned policies for a beam b by π . At any time t , the distribution of states for an executed policy π from time 0 to $t-1$ is represented by d_π^t . Furthermore, the average distribution of the states over a period T is

$$d_\pi = \frac{1}{T} \sum_{t=1}^T d_\pi^t \quad (17)$$

d) *Reward, R*: The reward determines how well an SU is performing on its beam b in the current network conditions. We measure the reward in terms of MOS, which represents the quality of experience (QoE). MOS value ranges from 0 to 5, where the value close to 5 (0) indicates that the SU is performing very well (very poor). The equation for the MOS is [16],

$$R = MOS = \frac{a_1 + a_2 FR + a_3 \ln(SBR)}{1 + a_4 TPER + a_5 (TPER)^2} \quad (18)$$

where FR, SBR and TPER are the frame rate, sending bitrate, and total packet error rate (calculated as $TPER = PER^2 + PDR^2 - PER * PDR$), respectively. The parameter a_i , $i \in \{1, 2, 3, 4, 5\}$ is estimated using the linear regression.

Main Components of FEAST: FEAST mainly consists of two parts: (1) Rapid Response Engine (RRE), and (2) Long Term Response Engine (LTRE) [19].

1) *Real-Time Decision Engine, RRE*: It performs the spectrum decision rapidly in real-time based on the best action chosen from the SVM-based predictions managed by LTRE module. If the observed reward (viz MOS) at instance t , is

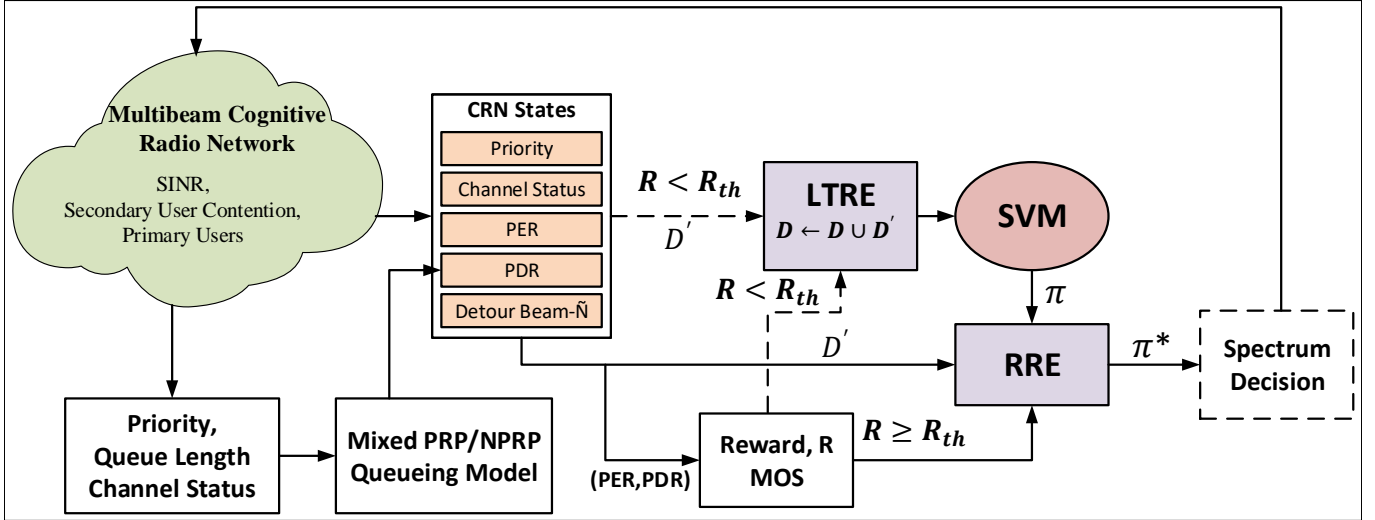


Fig. 6: FEAST based CBH for CRN, which mainly consists of SVM, LTRE, and RRE blocks to take the long term and short term decisions.

Algorithm 1 : FEAST-based spectrum decision scheme

Initialization, $D \leftarrow \emptyset$ and **Repeat**

Part-I: LTRE

Input: D' : RF State vector, $\{\rho_b^{(k)}, \chi_b^{(k)}, v_b^{(k)}, \delta_b^{(k)}, \tilde{N}_b^{(k)}\}$

Output: SVM: Decision model for RRE.

- 1: **if** $|D| > \text{MAXIMUMINSTANCES}$ **then**
- 2: Remove oldest Instance, \tilde{D} from D
- 3: **end if**
- 4: $D \leftarrow D \cup D'$ % Append current instance to D
- 5: $\text{MOS} = \text{SVM}(L, D) = \mathbf{w} \cdot \mathbf{x} + \mathbf{c}$ % Retrain the model
- 6: **TRANSFER** updated SVM to RRE

Part-II: RRE

Input: D' : RF State vector, $\{\rho_b^{(k)}, \chi_b^{(k)}, v_b^{(k)}, \delta_b^{(k)}, \tilde{N}_b^{(k)}\}$

Input: τ : Error threshold on MOS

Input: Updated SVM model, newSVM

Output: Optimal policy, π^*

- 1: $\text{SVM} \leftarrow \text{newSVM}$ % Receive newSVM from LTRE
- 2: Obtain new state observation, D'
- 3: **if** $|\text{MOS}_{t-1} - \text{MOS}_t| > \tau$ **then**
- 4: Trigger LTRE to Retrain
- 5: **end if**
- 6: **for** $a \in A$ **do**
- 7: $\pi_a = \text{SVM}(D', a)$ % prediction on each action
- 8: **end for**
- 9: $\pi^* = \text{argmax}(a, \pi_a)$ % Optimal Policy
- 10: **End**

below the threshold value (R_{th}), the RRE instructs LTRE to retrain the SVM model, based on the collected feature vectors. Then RRE compares the new action with the current model, and selects a suitable action with the best model.

2) *Long-Term Decision Engine, LTRE*: Long-term response model updates the learning model by collecting the network parameters as mentioned before. This model collects the newly observed network conditions (such as PDR, PER etc.) into its database and updates the SVM model. This model mainly

performs two functions: (1) Collect and add the new network conditions (i.e., feature vector, D') to its old dataset $D \leftarrow D \cup D'$, and (2) Calculate the new kernel values (i.e., compute the hyperplane), and update the SVM model using (19), which is then used by the RRE to perform the spectrum decisions. To avoid the dataset overflow, the old dataset is overwritten with feature vectors circularly after the data acquisition bound is reached.

Figure 6 illustrates our FEAST-based CBH model in CRN. Each beam observes both time varying and space varying channel variations in cognitive radio. Based on the observed channel variations, each beam of SU collects CRN states and uses them as feature vectors D' . In the beginning, the feature vectors are fed to LTRE as $D \leftarrow D \cup D'$ to build the decision model, π_a . This model is used by RRE to perform handoff decision. If the MOS falls below the threshold, R_{th} , the observed state vector D' is added to the feature stack, D and the model is retrained and updated at LTRE. The performance of the updated policy is compared with the old policy and the optimal policy π^* is used as the best policy for each state vector and action pair, and the process continues.

Algorithm 1 illustrates the pseudocode of FEAST model. At time instance t , a SU in beam b chooses an action $a \in A$ for an observation, D' , to maximize the performance of the spectrum decision (in terms of MOS) by using the learned model as follows:

$$\pi_a = \text{SVM}(D', a) = \sum_{sv=1}^{N_{sv}} (\alpha_{sv} - \alpha_{sv}^*) \phi(x_{sv}, x) + c \quad (19)$$

Here, α_{sv} and α_{sv}^* are the Lagrange multipliers, N_{sv} is the number of support vectors, and $\phi(x_{sv}, x)$ is the kernel, a non-linear mapping which transforms RF features to a high-dimensional space and gives a linear separation to get a perfect hyperplane if the feature vector observed at instance t is non-linear. x_{sv} is an instance in the training data, selected as a support vector to define the hyperplane, and x is the instance we attempt to predict using the learned model.

When the drop in MOS value is above τ , the RRE selects

the best policy which achieves the highest MOS, as follows:

$$\pi^* = \operatorname{argmax}(a, \pi_a), \quad a \in A \quad (20)$$

VII. PERFORMANCE ANALYSIS

In this section, we evaluate the performance of: (i) Mixed PRP/NRP M/G/1 queueing model in terms of the average queueing delay specifying how long a beam waits when it is interrupted by the high priority users; (ii) Beam handoff in terms of packet detouring; and (iii) The proposed FEAST model by integrating the "channel+beam" handoff scheme. The performance of our FEAST model is also compared with our previous learning-based spectrum handoff schemes (the reinforcement learning (RL) [1], apprenticeship learning (AL) [7], and multi teacher apprenticeship learning (MAL) [9].

In our simulations, we consider 3 PUs and 8 SUs, which communicate over 3 channels. Each SU is equipped with an MBSA having 8 beams with beamwidth of 45° , whereas PUs are equipped with an omni-directional antenna. We assume each node is experiencing Rician fading channel conditions [20], with atleast one line of sight (LOS) signal component, and the channel capacity is determined as in (5). To determine the PDR due to queueing delay, we use the equation (19) from [1] and the PER is varied from 2% – 10% with the packet size of $L_p = 1500$ bytes. The slot duration is $L_t = 50ms$. When the interference takes place, the sender SU uses other beams or channels to forward the interrupted data to the destination SU through relay node(s).

A. Average Queueing Delay

We evaluate the performance in terms of the average queueing delay (spectrum handoff delay) upon interruption from a PU or high priority SUs. Different priorities are assigned to the SUs depending on the delay constraint of their flow. The highest priority (priority = 1) is assigned to the interactive voice data with rate of $50Kbps$ and strict delay constraint of $50ms$. Priority 2 is assigned to the interactive Skype call with rate of $500Kbps$ and delay constraint of $100ms$. Priority 3 is assigned to the video-on-demand streaming data with rate of $> 1Mbps$ and delay constraint of $1sec$. Finally, the lowest priority (priority = 4) is assigned to the data without any delay constraint (e.g., file download). Since the SU priorities depend on the delay requirements of their data, we describe the channel access as a priority-based queueing model.

Figures 7a and 7b compare the average delay of the mixed PRP/NRP queueing model with the NPRP and PRP models, respectively, for different traffic classes (priorities). Here, the PU arrival rate is set to $\lambda_p = 0.05$ arrival/slot and its service rate is set to $E[Xp] = 6$ slots/arrival, and $E[Xs] = 5$ slots/arrival is set as the service rate for SU. We observe that the mixed PRP/NRP queueing model serves as a fair scheduling model, because it gives more spectrum access to the higher priority SUs by interrupting only those low priority SUs whose remaining service time is above a threshold determined by the discretion rule. As a result, the low priority SUs which are close to completing their service

are not interrupted. On the other hand, the NPRP queueing model does not allow the higher priority SUs to interrupt the lower priority SUs at all. As a result, the higher priority SUs experience slightly higher average delay and lower priority SUs experience lower average delay, compared to the mixed PRP/NRP queueing model. In the PRP model, the lower priority SUs suffer from higher queueing delay due to the frequent interruptions from higher priority SUs.

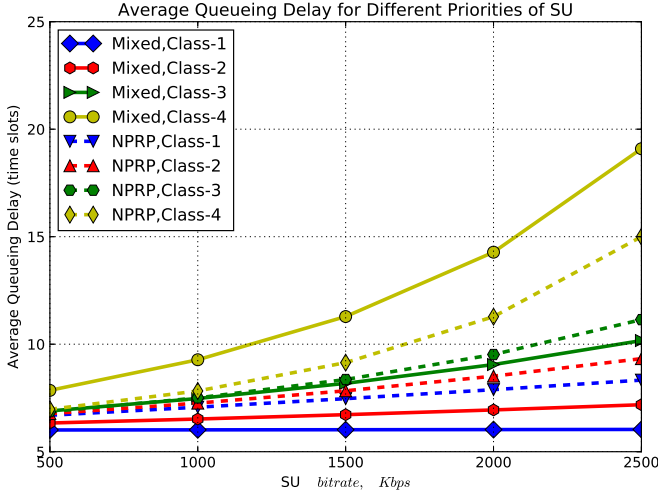
Figure 8 demonstrates the effect of the discretion threshold, ϕ , on average queueing delay, when ϕ is varied from 0 to 1. Here, $\phi = 0$ and 1 represent the NPRP and PRP modes, respectively, and $0 > \phi > 1$ represents the mixed PRP/NRP model. The queueing delay of the lowest priority SU (Priority 4) gets worse when the discretion threshold increases, because a higher-priority SU can easily interrupt it. Based on the traffic delay constraint, the parameter ϕ can be tuned to meet the QoS requirements of SUs.

B. Beam Handoff Performance

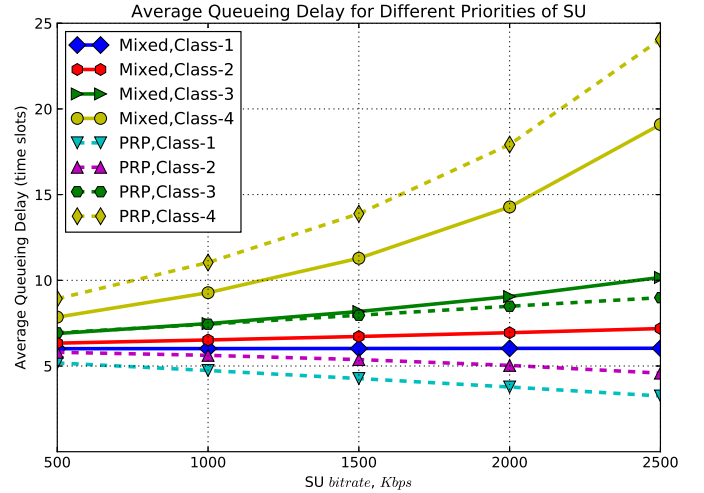
Figure 9 shows an ideal case where all the detour beams have the same available channel capacity for transmitting the detour packets. Here, the source data rate (r_b) is $3Mbps$. The plot shows the total data rate that can be achieved with different number of detour paths when each beam carries the same percentage of detoured source data. A higher data rate is obtained by either increasing the number of detour beams or the data carried on each beam, until 100% detour data is transmitted.

Figure 10 shows the variations in MOS for different types of source data, when each detour beam has a channel capacity of $C_i = 4.5Mbps$ and its own data rate is $R_i = 3Mbps$. In this case, four detour beams are available for forwarding the interrupted beam's data. The Priority 1 data of the interrupted beam (with source rate, $r_b = 50Kbps$, and delay deadline = $50ms$) is detoured with a high MOS score of 4 since it requires less channel capacity but also has stringent delay constraint. Also note that each packet on the detour beam travels through two hops which adds to the delay leading to the packet drops. The Priority 2 data of the interrupted beam (with source rate, $r_b = 500Kbps$, and delay deadline = $100ms$) is detoured with a slightly lower MOS. The Priority 3 data of the interrupted beam (with source rate, $r_b \geq 1000Kbps$, and delay deadline = $1sec$) achieves MOS value of lower than 3 because it requires more channel resources and doesn't enjoy any priority over the detour beam's own data which also has priority 3. An interesting trend is observed for the Priority 3 data, i.e., as the data rate increases the MOS also slightly increases. This is because MOS is logarithmically proportional to the source bit rate.

In Figure 11, the number of available detour beams as well as the source data rate is changed. Using more detour beams improves MOS score when the source data rate of the interrupted beam is $> 500Kbps$. When the data rate is high and more packets are detoured through a beam, packet drop rate increases due to the packet expiry in the queue over two hops. As the packets are distributed among more detour beams, the load on each beam is reduced leading to a lower PDR, which provides a higher MOS.



(a) NPRP v/s Mixed PRP-NPRP model



(b) PRP v/s Mixed PRP-NPRP model

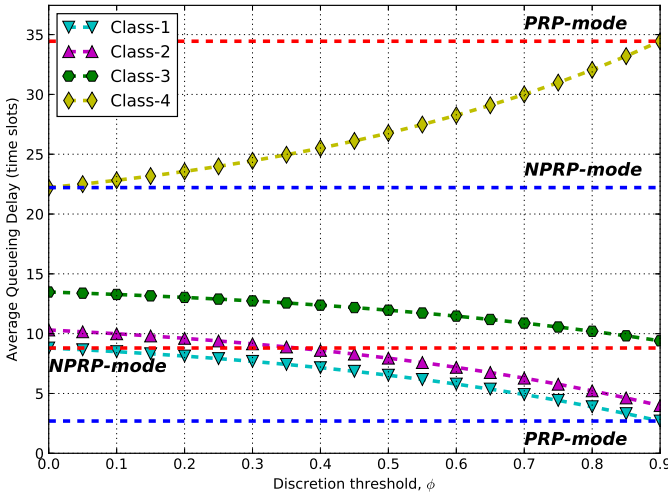
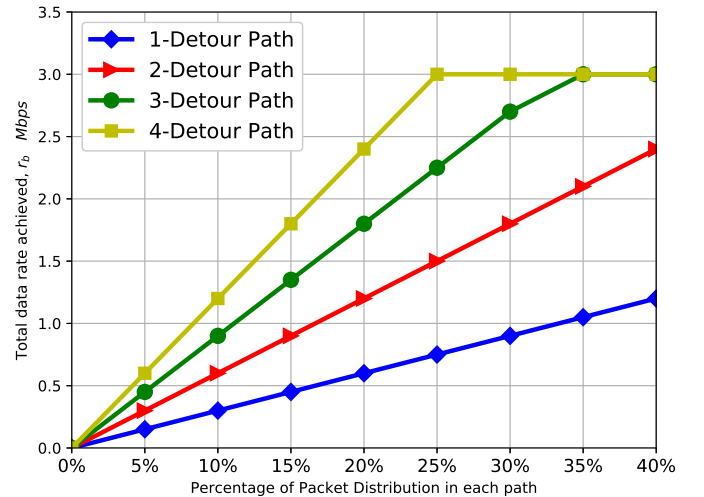
Fig. 7: The comparison of (a) Mixed PRP/NPRP vs. NPRP, and (b) Mixed PRP/NPRP vs. PRP queueing models, with $\lambda_p = 0.05$, $E[Xp] = 6$ slots, and $E[Xs] = 5$ slots.Fig. 8: Effect of discretion threshold, ϕ on the average queueing delay for different priorities of SUs.

Fig. 9: (Ideal case) Percentage of packet detour vs. achieved source data rate. Here, every beam has the same percentage of packet detouring and latency requirements.

Figure 12 shows the MOS score when both the source data rate, r_b , and each detour beam's own data rate, R_i , are varied over the range of 50Kbps to 3Mbps. Here, four detour paths are available. No variation in the performance is observed for the higher priority data, with data rates of 50Kbps (Priority 1 data) and 500Kbps (Priority 2 data), irrespective of the detour beam's own data rate, R_i . Similar trend is observed for the source rate of 1Mbps and 1.5Mbps, but the MOS score is lower because the source data priority is 3 which is the same as the detour beam's own data. Whereas, for the source rate $r_b \geq 2$ Mbps (which also corresponds to priority 3) and $R_i \geq 2$ Mbps, we observe a further drop in the MOS score because the load on each beam increases and the packets experience a higher delay (i.e., higher PDR).

C. FEAST-based Spectrum Decision Performance

We study performance of the cognitive spectrum decision using our machine learning based spectrum decision model, i.e.,

FEAST. We generate one feature vector at a time to train the *FEAST* model. A feature vector consists of PER, PDR, detour-status, channel-status, and flow priority. An observed feature vector can belong to one of the three classes: stay-and-wait, channel handoff, and beam handoff. In our simulations, the PER was varied from 2% to 10%, and PDR is calculated using the queueing model. The arrival rate and the service time of the SU and PU connections are set as $\lambda_p = 0.05$ arrivals/slot, $E[Xp] = 6$ slots/arrival, $\lambda_s = 0.05$ arrivals/slot, and $E[Xs] = 8$ slots/arrival. In addition, we consider the availability of three channels and four detour beams, and the number of traffic priority classes is 4. Based on the training model, the node takes the spectrum decisions with respect to the observed RF conditions. When there is a continuous degradation in the performance, the observed feature vector will be added to the feature set and the model is retrained.

Our main goal is to show that the proposed supervised

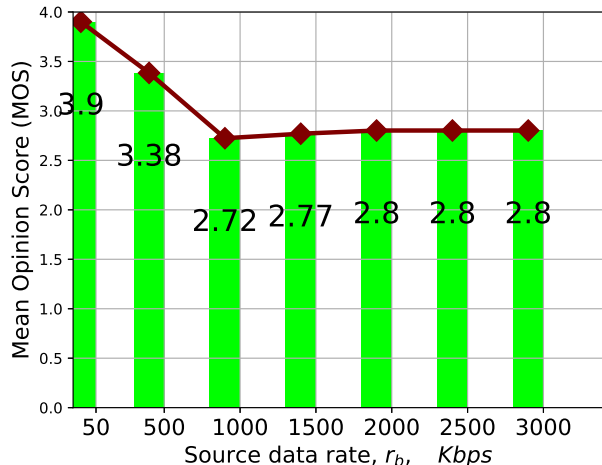


Fig. 10: MOS performance for different source rate r_b when each detour beam has a channel capacity of $C_i=4.5$ Mbps and it's own data rate $R_i=3$ Mbps.

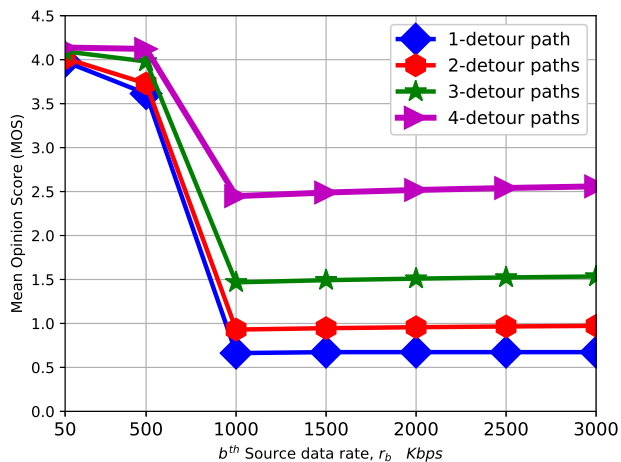


Fig. 11: MOS performance for different source rates and different numbers of detour beams. Each detour beam has channel capacity of $C_i=4.5$ Mbps and it's own data rate $R_i=3$ Mbps.

learning algorithm, FEAST, can outperform the unsupervised learning based schemes (e.g., RL, AL, and MAL), in terms of the number of iterations needed to achieve the optimal condition. Here, we consider an iteration as the packet transmission attempt and analyze the performance of our model by considering two scenarios: slow moving node and fast (random) moving node.

To compare different learning based schemes, we use the soft-max policy with temperature rate ($1/K$), where K is the number of iterations and discount rate $\gamma = 0.6$. The temperature value decreases with the number of iterations to make sure that the learning model goes through the exploration and exploitation phases for each state-action pair.

Figures 13a and 13b show the number of iterations needed for achieving the optimal performance (measured by MOS) for the traffic of four priorities for the slow-moving and fast-moving scenarios, respectively. For both the scenarios, the reinforcement learning (RL)-based spectrum decision [1] needs

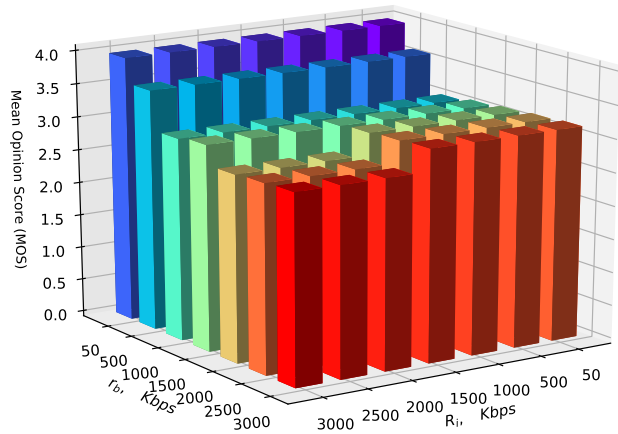


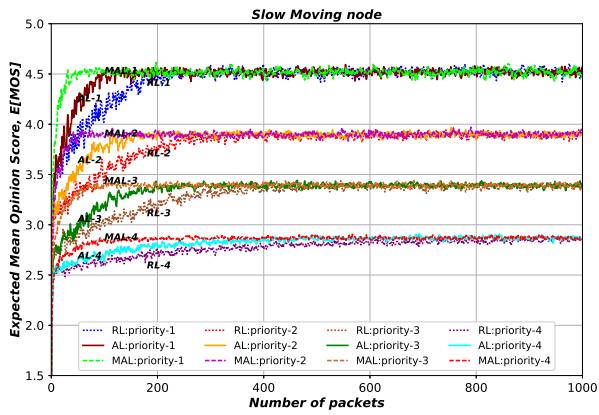
Fig. 12: MOS performance for different source rates, r_b and detour beam's own data rates, R_i

more than 200 iterations to converge. For the apprenticeship learning (AL)-based spectrum decision [7], the performance appears to be slightly better since the node achieves optimal performance within 200 iterations. The multi-teacher apprenticeship learning (MAL)-based spectrum decision [9] needs only about 50 iterations to reach the optimal performance. Further, the slow-moving SU needs less number of iterations to achieve the optimal performance compared to the fast-moving SU.

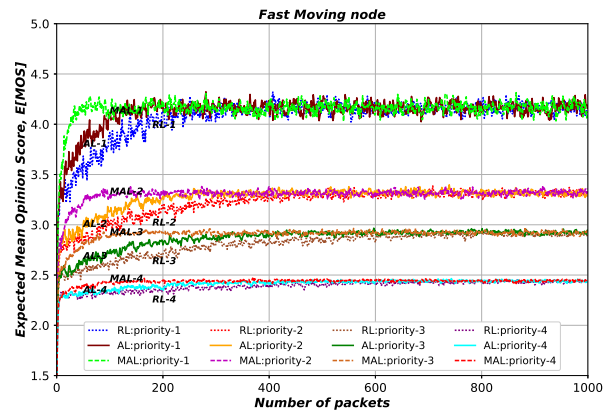
The performance of the proposed FEAST model-based spectrum decision scheme is shown in Fig. 14a (for slow-moving SU) and 14b (for fast-moving SU). The FEAST model based spectrum decision scheme needs only about 15 iterations to achieve the optimal MOS value for the traffic of all the four priorities. It is evident from Fig. 15b, which shows the zoomed version for FEAST and MAL [9] schemes for the first 100 iterations, that the FEAST model achieves a significant improvement compared to the MAL based model. In addition, the FEAST model also outperforms the No-FEAST model which uses no online learning ([14]) in Fig. 14a and 14b.

Note that the number of iterations taken by the spectrum decision scheme to converge to the optimal performance is very important for the SUs with delay sensitive traffic. Requiring more iterations for deciding the handoff would also degrade the performance (such as spectrum utilization and throughput) for dynamic channel conditions. More importantly, a CR node does not have much time for handoff operations since the availability of channel also varies with time. Although the AL and MAL do not require the exploration phase for each state-action pair, they need more time to search and receive the optimal strategy from multiple nodes, which affects the utilization of the available spectrum. The proposed FEAST model takes only a few iterations without the need for other node's information, unlike the MAL model.

Table I shows the confusion matrix for the spectrum decision schemes based on the FEAST and No-FEAST models, determined by using the actual labels (AL) and predicted labels (PL) for 1000 iterations. The True Positive (TP) values are

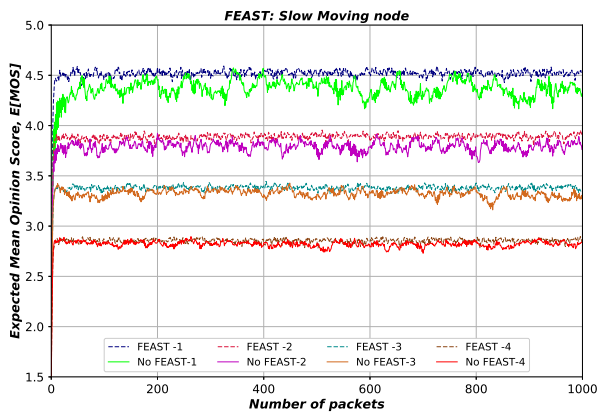


(a) Slow Moving Node

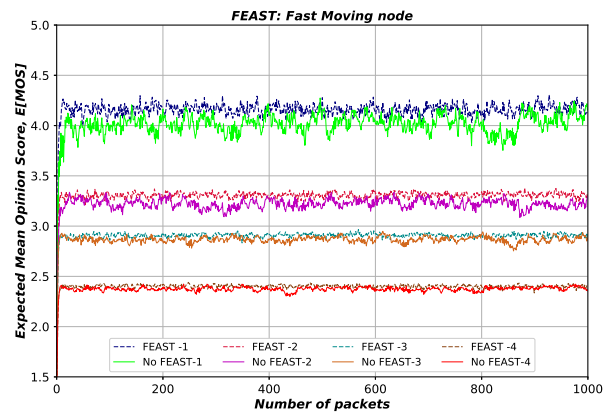


(b) Fast Moving Node

Fig. 13: Performance comparison of our previously reported learning schemes, RL, AL, and MAL.

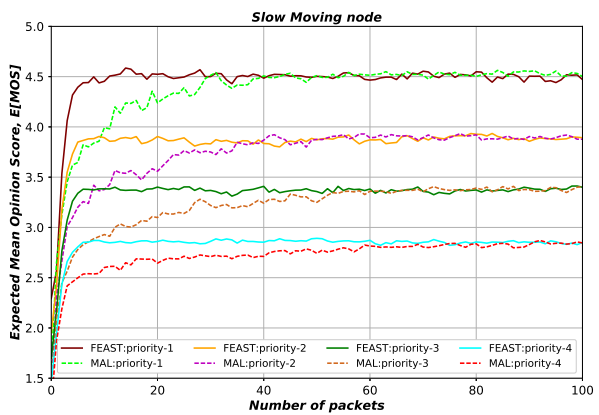


(a) Slow Moving Node

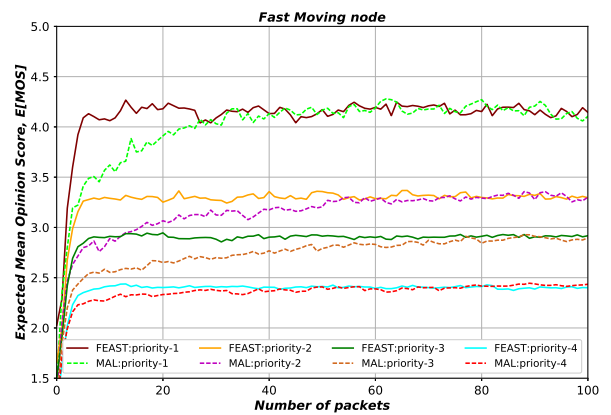


(b) Fast Moving Node

Fig. 14: Performance analysis of the FEAST model based spectrum decision scheme.



(a) Slow Moving Node



(b) Fast Moving Node

Fig. 15: Performance comparison of FEAST model based spectrum decision scheme with MAL-based scheme for 100 iterations (packet transmission).

PL \ AL		Stay-and-Wait	Channel Handoff	Beam Handoff
Stay-and-Wait	FEAST	246	2	1
	No-FEAST	142	97	76
Channel Handoff	FEAST	2	211	3
	No-FEAST	108	135	81
Beam Handoff	FEAST	3	5	527
	No-FEAST	103	73	185

TABLE I: Confusion matrix comparison between the FEAST (online learning) and No-FEAST (no-online learning) models.

along the diagonal direction and the off-diagonal elements represent the False Positive (FP) and False Negative (FN) values. To compute the confusion matrix, the predicted labels from all three folds are combined into one vector, and compared to the actual labels of the dataset. In the FEAST model, 984 out of 1000 predictions are TP for all the three classes. While in the No-FEAST model [14], the total number of TPs are only 491, which is less than 50% of the actual predictions, exemplifying the need for online learning. When adding a new feature D' to the feature stack, $D \leftarrow D \cup D'$, if the number of feature vectors belonging to one class dominates the feature vectors of other classes, the model will be biased towards the dominant class. Therefore, maintaining an equal proportion of feature vectors for each class during data aggregation can reduce the risk of the model being biased towards a particular class.

Finally, Fig 16 demonstrates the number of support vectors (SVs) used during spectrum decision process for the traffic of four priority classes. The number of SVs increases almost monotonically with the number of training vectors (counted in terms of the number of packet transmissions), strengthening the decision boundary for each class.

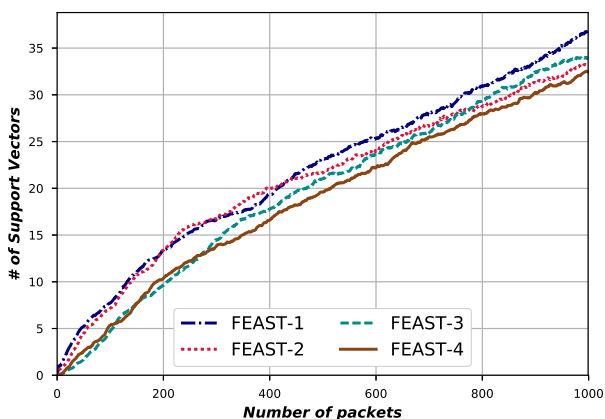


Fig. 16: Number of support vectors generated in the FEAST model.

VIII. CONCLUSIONS

We designed a novel FEAST-based "channel + beam" handoff control scheme for MBSA-based CRNs. FEAST uses an SVM-based online supervised learning scheme. By using the independent and parallel, mixed PRP/NPRP M/G/1

queueing model with a discretion rule, the average waiting delay experienced during the interruption of a beam was determined. During the waiting time, the interrupted beam's data was detoured through the neighboring beams over 2-hop paths by using a novel beam handoff scheme. The beam handoff performance was analyzed using MOS by varying the source data rate as well as the detouring beam's own data rate. Performance analysis showed that more detouring paths with enough detouring rate can help to achieve the optimal performance. The extension of spectrum decision to the online learning model (i.e., FEAST) significantly enhanced the spectrum decision performance. Our model significantly outperformed the unsupervised learning based handoff control schemes, in terms of the expected MOS and it also needed far less iterations to achieve the optimal condition, in the presence of dynamic channel and network conditions.

REFERENCES

- [1] Y. Wu, F. Hu, S. Kumar, Y. Zhu, A. Talari, N. Rahnavard, and J. D. Matyjas, "A learning-based QoE-driven spectrum handoff scheme for multimedia transmissions over cognitive radio networks," *IEEE J. Selected Areas in Comm.*, vol. 32, no. 11, pp. 2134–2148, 2014.
- [2] Y. Zhang, X. Li, and M. G. Amin, "Multi-channel smart antennas in wireless networks," in *40th IEEE Asilomar Conf. on Signals, Systems and Computers*, 2006, pp. 305–309.
- [3] A. Koushik, F. Hu, and S. Kumar, "Multi-Class "Channel+ Beam" Handoff in Cognitive Radio Networks with Multi-Beam Smart Antennas," in *IEEE Global Comm. Conf. (GLOBECOM)*, 2016, pp. 1–6.
- [4] Y. Z. Cho and C. K. Un, "Analysis of the M/G/1 queue under a combined preemptive/nonpreemptive priority discipline," *IEEE Trans. Comm.*, vol. 41, no. 1, pp. 132–141, 1993.
- [5] A. Chattopadhyay and A. Chockalingam, "Past queue length based low-overhead link scheduling in multi-beam wireless mesh networks," in *Intl. Conf. Signal Processing and Comm. (SPCOM)*, 2010, pp. 1–5.
- [6] B. K. Chalise, Y. D. Zhang, and M. G. Amin, "Multi-beam scheduling for unmanned aerial vehicle networks," in *IEEE/CIC Intl. Conf. Comm. in China (ICCC)*, 2013, pp. 442–447.
- [7] Y. Wu, F. Hu, S. Kumar, J. Matyjas, Q. Sun, and Y. Zhu, "Apprenticeship learning based spectrum decision in multi-channel wireless mesh networks with multi-beam antennas," *IEEE Trans. Mobile Computing*, vol. 16, no. 2, pp. 314–325, 2017.
- [8] L.-C. Wang, C.-W. Wang, and C.-J. Chang, "Modeling and analysis for spectrum handoffs in cognitive radio networks," *IEEE Trans. Mobile Computing*, vol. 11, no. 9, pp. 1499–1513, 2012.
- [9] Y. Wu, F. Hu, Y. Zhu, and S. Kumar, "Optimal Spectrum Handoff Control for CRN Based on Hybrid Priority Queuing and Multi-Teacher Apprenticeship Learning," *IEEE Trans. Vehicular Technology*, vol. 66, no. 3, pp. 2630–2642, 2017.
- [10] K. Wu, L. Guo, H. Chen, Y. Li, and J. Lin, "Queueing based optimal scheduling mechanism for QoE provisioning in cognitive radio relaying network," in *16th Intl. Symp. Wireless Personal Multimedia Comm. (WPMC)*, 2013, pp. 1–5.
- [11] K. Jitvanichphaibool, Y.-C. Liang, and R. Zhang, "Beamforming and power control for multi-antenna cognitive two-way relaying," in *IEEE Wireless Comm. and Networking Conf.*, 2009, pp. 1–6.
- [12] A. Koushik, F. Hu, J. Qi, and S. Kumar, "Cognitive Spectrum Decision via Machine Learning in CRN," in *Conf. Information Technology New Generations*. Springer, 2016, pp. 13–23.
- [13] J. Guo, H. Ji, Y. Li, and X. Li, "A novel spectrum handoff management scheme based on SVM in cognitive radio networks," in *6th Intl. ICST Conf. Comm. and Networking in China (CHINACOM)*, 2011, pp. 645–649.
- [14] Y. Wang, Z. Zhang, L. Ma, and J. Chen, "SVM-based spectrum mobility prediction scheme in mobile cognitive radio networks," *The Scientific World J.*, 2014.
- [15] C. Zhang, X. Wang, and J. Li, "Cooperative cognitive radio with priority queueing analysis," in *IEEE Intl. Conf. Comm.*, 2009, pp. 1–5.
- [16] F. Ribeiro, D. Florêncio, C. Zhang, and M. Seltzer, "Crowdmoss: An approach for crowdsourcing mean opinion score studies," in *IEEE Intl. Conf. Acoustics, Speech and Signal Processing (ICASSP)*, 2011, pp. 2416–2419.

- [17] E. Byvatov, U. Fechner, J. Sadowski, and G. Schneider, "Comparison of support vector machine and artificial neural network systems for drug/nondrug classification," *J. Chemical Information and Computer Sciences*, vol. 43, no. 6, pp. 1882–1889, 2003.
- [18] O. P. Awe, Z. Zhu, and S. Lambotharan, "Eigenvalue and support vector machine techniques for spectrum sensing in cognitive radio networks," in *Conf. Technologies and Applications of Artificial Intelligence (TAAI)*, 2013, pp. 223–227.
- [19] K. Z. Haigh, A. M. Mackay, M. R. Cook, and L. L. Lin, "Parallel Learning and Decision Making for a Smart Embedded Communications Platform," 2015, accessed on April 10, 2017. [Online]. Available: <http://www.cs.cmu.edu/khaigh/papers/2015-HaighTechReport-SO.sm.pdf>
- [20] M. L. Moher and J. H. Lodge, "TCMP-A modulation and coding strategy for Rician fading channels," *IEEE J. Selected Areas in Communications*, vol. 7, no. 9, pp. 1347–1355, 1989.